Numerical Study of Cone Penetration in Calcareous Sands: Investigating Cone Tip Resistance Correction Factors for Crushable Soils

Stephanie Hyder, P.E.[1] and *Diane* Moug, Ph.D.[2]

[1]*M.S. Student, Department of Civil and Environmental Engineering, Portland State University,*
1930 SW 4th Ave., Suite #200, Portland, Oregon, United States of America
[2]*Assistant Professor, Department of Civil and Environmental Engineering, Portland State University,*
1930 SW 4th Ave., Suite #200, Portland, Oregon, United States of America
[#]*Corresponding author: steffhyder@gmail.com*

ABSTRACT

The cone penetration test (CPT) is used to characterize the behaviour and properties of soils, including the cyclic strength against earthquake liquefaction triggering. The cone tip resistance relates to cyclic strength through relative density, where relative density is closely related to both cone tip resistance and liquefaction susceptibility. Currently, published methods of estimating liquefaction potential (i.e., cyclic resistance ratio) are based on silica sands and do not properly characterize calcareous sands. The measured cone tip resistance in calcareous sands is lower than in silica sands at the same relative density; this difference is generally attributed to the higher compressibility of calcareous sands due to particle crushing during cone penetration. Consequently, application of CPT-based liquefaction triggering evaluations in calcareous sands result in over-conservative analysis. To avoid over-conservative analysis, projects may develop site-specific correction factors to adjust the cone tip resistance in calcareous sand to the equivalent value in silica sand at the equivalent relative density. This study aims to investigate cone penetration in calcareous sands compared to silica sands by examining the roles of soil compressibility and other fundamental soil parameters. The study is performed with a direct axisymmetric penetration model and the MIT-S1 constitutive model calibrated against published mechanical behaviour for a calcareous sand; the simulated cone penetration results are compared with simulated cone penetration in Ottawa F-65 sand. Compressibility of the calibrations is adjusted to explore the role of compressibility on cone tip resistance. The numerical results show that differences in compressibility only partially account for differences in cone tip resistance between calcareous and silica sands at the same initial state. However, the results support that critical state line position does strongly relate to differences in cone tip resistance between the two soil types. The study results provide a basis to investigate differences in critical state line position as a basis for site-specific cone tip resistance correction factors for calcareous soils.

Keywords: Cone penetration test; CPT; finite difference analysis; numerical analysis; numerical modelling; calcareous sands.

1. Introduction

Calcareous sands, also known as carbonate or coral sands, are often present in geotechnical engineering applications in near shore, offshore, and dredged fill environments. These sands are classified separately from “standard” silica sands due to their origin and carbonate content. They are more brittle in nature, have porous grains and abrasive grain surfaces due to the carbonate content, and consequently have different mechanical properties than siliceous sands.

A common method for characterizing sand profiles is the cone penetration test (CPT). CPT is useful for soil state characterization (e.g., relative density) and state-dependent property characterization (e.g., peak friction angle, cyclic resistance ratio) of granular soils that are otherwise difficult to sample intact.

Carbonate sand CPT tip resistances (q_t) are typically about 25% lower than silica sands while at the same relative density (*Dr*) (Debats et al. 2015). For most sand parameter interpretation from CPT, published correlations and charts are based on empirical data from silica sands (e.g., Salgado et al. 1997, Mayne 2007). This can lead an engineer to classify a calcareous sand as having a high liquefaction hazard or low shear strength due to underestimation of its *Dr* with CPT-based methods.

A correction factor for calcareous sands, called the shell correction factor (SCF), is often applied to q_t for calcareous sands to estimate the equivalent q_t for a silica sand at the same *Dr*:

$$SCF = q_{t,silica} \div q_{t,calcareous} \tag{1}$$

Al-Homoud et al. (2006) developed SCF as a function of *Dr*; the larger the *Dr*, the larger of correction needs to be applied:

$$SCF = 0.0046 \times Dr\,[\%] + 1.3629 \tag{2}$$

Current practice is to develop site-specific SCF, which is a burdensome task largely due to the equipment needed to characterize the relationship between q_t and *Dr*, which typically involves either a calibration chamber or geotechnical centrifuge. Calibration chambers present several expensive problems: they require around one ton of sand per tested *Dr*, few densities can be tested in a reasonable amount of time, and measurement corrections on the chamber introduce uncertainty (Debats et al 2018). Whereas geotechnical centrifuges are specialized equipment available to a limited number of labs. Motivated by the expense of site-specific SCF, this study examines fundamental differences between calcareous sand silica sands that may account for differences in q_t at the same *Dr*.

The higher compressibility of calcareous sands compared to silica sands is often used to explain the need for SCFs (e.g., Al-Homoud et al. 2006, Debats et al. 2015). Other studies (e.g., Moug et al. 2019a) show that differences of q_t can often be attributed to critical state line (CSL) position, which is partially related to soil compressibility. This study tests two hypotheses regarding calcareous and silica sands: differences in compressibility are related to differences in q_t, and differences in CSL position relate to differences in q_t.

To analyze q_t in calcareous sands, cone penetration was simulated using a direct axisymmetric cone penetration model in FLAC 8.0 (FLAC, Itasca 2016) with the MIT-S1 constitutive model (Pestana & Whittle 1999) calibrated for the calcareous sand behaviour in Giretti et al. (2018a,b). This paper presents calibration of the MIT-S1 model, cone penetration simulations of the model, plus discussion, analysis, and comparison of the current SCF and our suggested modified approach.

2. Cone Penetration Model & Soil Model Calibration

2.1. Direct axisymmetric penetration model

Drained cone penetration is simulated with a direct axisymmetric penetration model in FLAC 8.0. Large deformations around the penetrating cone are accommodated by a user-defined Arbitrary Lagrangian Eulerian rezoning and remapping algorithm. This cone penetration model and ALE algorithm is presented and validated in Moug et al. (2019b).

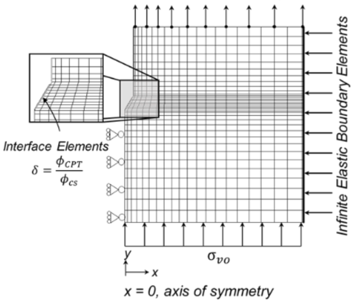

Figure 1. FLAC direct axisymmetric model (from Moug et al. 2019b).

The model captures penetration for a 3.57 cm diameter cone (standard 10 cm^2 cone). A simplified illustration of the model boundary conditions is shown in Fig. 1. The model dimensions are 30 cone diameters in the x-direction, 22.5 cone diameters in the y-direction below the cone tip, and 5 cone diameters in the y-direction above the cone shoulder. The in-situ vertical stress condition is applied at the bottom boundary; penetration velocity is applied to gridpoints at the top boundary; and an infinite elastic boundary condition is applied to gridpoints at the far radial boundary. Interface conditions between the soil and cone are captured with Mohr-Coulomb interface elements with a coefficient of friction of 0.6 to capture similar conditions as used for Ottawa F-65 sand simulations in Moug et al. (2019b).

Cone penetration is simulated from a wished-in-place condition at the depth of interest. Then, cone penetration is simulated as soil moving upward relative to a stationary cone until steady-state stress conditions around the cone tip are reached. For this study, all simulations were run, at minimum, for the equivalent of 20 cone diameters of penetration to reach steady-state conditions.

2.2. MIT-S1 Model Calibration

MIT-S1 is a bounding surface plasticity model developed by Pestana and Whittle (1999) that can capture a wide range of soil behaviours from clays to sands. The model was implemented in FLAC by Jaeger (2012) with additional modifications as described in Moug (2017).

The MIT-S1 model was calibrated for the M1 sand presented in Giretti et al. (2018a,b). The sand in their studies was obtained from dredged artificial islands in the United Arab Emirates. M1 was reported to be 97% carbonate with a fines content of 5%, sand content of 91%, and 4% gravel content. The M1 data used for parameter calibration included data from compression tests, drained triaxial compression tests, and cone penetration in a geotechnical centrifuge and calibration chamber.

Calibration of the MIT-S1 model for cone penetration followed the approach in Moug et al. (2019a), prioritizing calibration of compression behaviour and CSL position to capture reasonable q_t values. The calibrated MIT-S1 parameter values for M1 sand, along with a brief description of the model parameters, are shown in Table 1. The MIT-S1 model parameters for Ottawa F-65 sand (OS) are also presented in Table 1 since the simulated results of M1 calcareous sand will be compared against OS; calibration and validation of OS are presented in Moug et al. (2019a).

Compression behaviour of MIT-S1 is modelled with the limiting compression curve (LCC). The LCC represents a linear line in log void ratio (e) – log effective stress space that the sand compression path follows at high stresses and in the particle crushing regime (Pestana & Whittle 1995). Compression parameters σ'_{vref}, ρ_c, and θ were calibrated from one-dimensional compression test data from Giretti et al. (2018a), as shown in Fig. 2. The LCC of M1 sand was fit to the compression behaviour at high stresses (i.e., for $\sigma'_v > 10$ MPa) with ρ_c and σ'_{vref} while θ was adjusted to approximate the soil's transition to the LCC.

Table 1. MIT-S1 Calibration input parameters for M1 calcareous sand and Ottawa sand.

Description		Calibrated Parameters	
		M1	**OS^a**
ρ_c	LCC slope shown in log(e)-log(p')	0.37	0.49
φ'_{cs}	Critical state friction angle	37	30
φ'_{mr}	Peak friction angle at e = 1	36.5	18.2
σ'_{vref}	Reference σ'_v at e = 1 on the 1-D LCC	45	129
p_φ	Controls variation of peak friction angle with e	0.6	2.6
m	Controls shape of yield and bounding surfaces	0.75	0.67
K_{0NC}	Lateral earth pressure coefficient	0.5	0.5
Cb	Controls small strain elastic moduli	750	750
μ'_0	Poisson's ratio (small strain, load reversal)	0.23	0.23
ω	Controls nonlinearity in Poisson's ratio	1.0	1.0
ω_s	Controls nonlinearity of elastic moduli in shear	2.5	2.5
ψ	Controls rate of evolution of yield surface anisotropy	50	50
Θ	Transition to LCC for compression behaviour	0.6	0.6

^{a}*calibration parameters from Moug et al. 2019b*

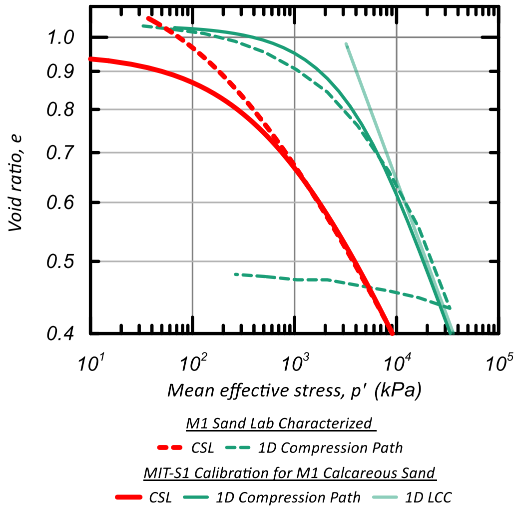

Figure 2. CSL, LCC and compression behaviour of M1 sand. Lab-measured 1D compression behaviour and lab-characterized CSL are from Giretti et al. (2018a).

The CSL was explicitly fit to drained triaxial compression (TX) lab data using φ'_{cs}, φ'_{mr}, m, and p_φ. The LCC parameters also affect the CSL position in void ratio – mean effective stress (e-p') space. As shown in previous studies, soil around the penetrating cone is loaded to critical state conditions, therefore, the CSL position strongly relates to q_t (e.g., Moug et al. 2019b, Moug & Price 2023). Therefore, calibrating the MIT-S1 CSL to be comparable to the laboratory-characterized CSL was the priority for calibration, with less priority placed on capturing other soil behaviours when compromise was necessary. Fig. 2 compares the MIT-S1 calibrated CSL with the CSL interpreted in Giretti et al. (2018a). A limitation of the MIT-S1 model for this application is that the CSL position is fixed, whereas Ciantia et al. (2019) show that the CSL position and shape in e-p' space changes with particle crushing. Other model parameters, including ψ, Cb, μ'_0, ω, and ω_s, were based on the OS calibration and standard soil values.

The shear behaviour of the M1 sand calibration is compared against the laboratory drained TX data (2018a) in Fig. 3 and Fig. 4 using single element drained TX simulations in FLAC. Fig. 3 shows the TX paths in e-p' space for both lab data and the MIT-S1 calibration. For the same initial conditions, the paths have similar contractive and dilative tendencies and reach a similar p' at critical state. However, for soils that are initially dense of the critical state line (i.e., below the CSL), the calibrated behaviour does not have as strong of an initial contraction as the laboratory-measured behaviour.

Fig. 4 compares the simulated and lab-measured stress ratio during TX from the same initial conditions; the figure plots the stress ratio (η), which is the ratio of deviatoric stress (q) to p', versus axial strain. While the simulations converge at a similar η to the lab data, there is a lack of peak in η and generally a softer response compared to the lab data. This behaviour was difficult to capture in the MIT-S1 model while still prioritizing the shape and position of the CSL and LCCs, possibly due to limitations of the CSL changing with particle crushing, as discussed above.

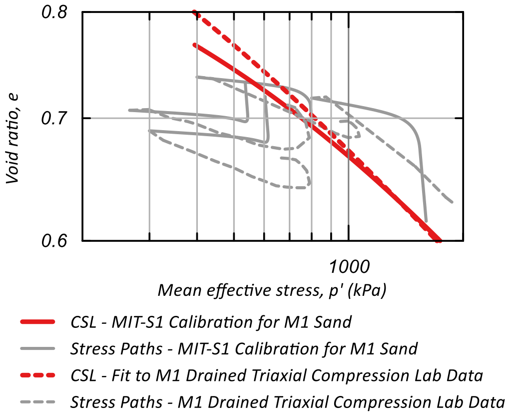

Figure 3. Drained TX stress paths and CSL. MIT-S1 calibration and M1 lab data.

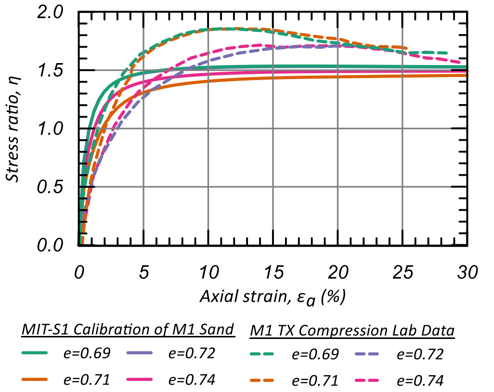

Figure 4. Simulated and lab-measured stress ratio during TX from the same initial conditions versus axial strain.

Typically, calcareous sands are more dilative in shear loading than silica sands; this is consistent between the M1 lab data and OS sand calibration as shown in Fig. 5 by the difference between peak friction angle (φ_{pk}) and φ_{cs} versus the state parameter (ξ), where the M1 lab data consistently plots higher than the OS data. Although the OS sand data in Fig. 5 is a simulated behaviour, this behaviour was calibrated to be consistent with the φ_{pk}-φ_{cs} versus ξ relationship by Jeffries and Been (1985). ξ, as defined by Jeffries and Been, is the difference between the current e and critical state void ratio (e_{cs}), or the vertical distance from e to the CSL in e-p' space.

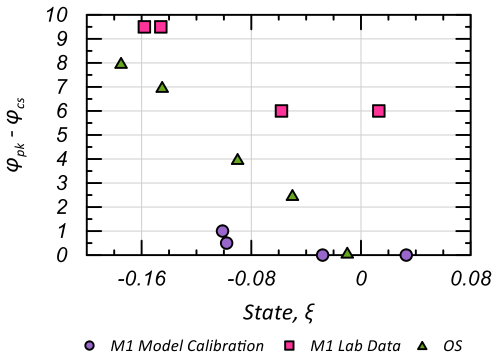

Figure 5. φ_{pk}–φ_{cs} versus ξ. MIT-S1 M1 calibration, M1 lab data, and MIT-S1 OS calibration.

The simulated M1 behaviour consistently plots below the simulated OS and lab M1 behaviour in Fig. 5, illustrating a limitation in the model to capture dilativity in calcareous sands. Despite these limitations, cone penetration behaviour was generally well-captured and informative to the objectives of the study, as will be discussed in the following sections.

2.3. Validation of simulated cone penetration in calcareous sand

Cone penetration simulations were performed using FLAC at e=0.63, 0.66, 0.70, and 0.78 with the M1 parameters shown in Table 1 and a range of vertical effective stresses (σ'_v) to represent different depths of a soil profile. q_t versus σ'_v of M1 simulations compared against M1 centrifuge data from Giretti et al (2018b) is shown in Fig. 6. The cone penetration model captures q_t well with some limitations at e=0.70 for higher σ'_v. These differences are attributed to variability in the calibration chamber, soil preparation, and other testing variability. Generally, the trend of q_t with decreasing e and increasing σ'_v measured from cone penetration in a geotechnical centrifuge is approximated by the simulations.

Fig. 7 shows simulated M1 (blue circles) and OS (red circles) q_t from ξ=-0.15 to 0.0. These simulations were performed at σ'_v=100 kPa. As expected, q_t increases with decreasing ξ. Overall, the q_t of M1 (q_{tM1}) are lower than the simulated OS (q_{tOS}).

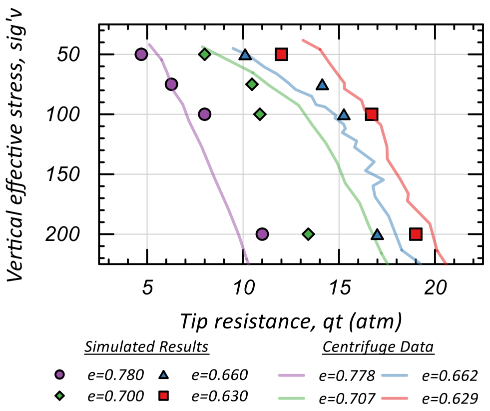

Figure 6. q_t from direct penetration simulations in M1 sand compared to M1 centrifuge data.

Validation of the M1 calibration to capture calcareous sand behaviour during cone penetration is also performed by comparing the equivalent SCF with published values. The ratio between q_{tOS} and q_{tM1} versus ξ are plotted in Fig. 8, which would be the SCF for these two soils. The trend of SCF from the simulated results are consistent with reported values. Jamiolkowski and Pasqualini (1992) report that SCF increases as Dr increases with SCF≈1.5 for Dr=50-70% and SCF≈2.0 for Dr=90%. This trend is reproduced by the results in Fig. 8; q_{tOS}/q_{tM1}=1.6 for ξ=-0.05 and q_{tOS}/q_{tM1}=1.9. for ξ=-0.15. The differences of simulated q_t between M1 and OS are similar to published differences, therefore supporting that the primary soil parameters affecting q_t in calcareous sand are captured with the MIT-S1 M1 calibration.

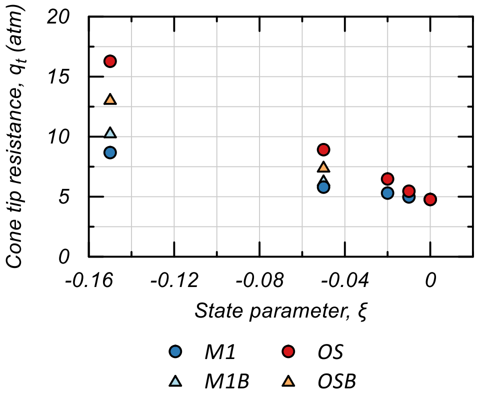

Figure 7. Simulated relationship between q_t and ξ for M1 and OS sands. "B" calibrations have M1 and OS parameters with the compressibility parameters changed to the other soil type.

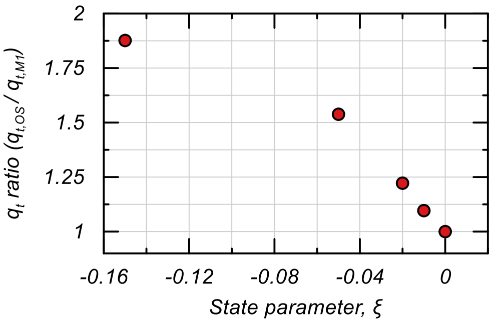

Figure 8. Change of q_t ratio [equivalent SCF] for M1 and OS with ξ.

3. Analysis

3.1.1. Role of compressibility on q_t

The relationship between soil compressibility and q_t was examined by simulating cone penetration in the calibrated OS and M1 sands as presented above, and with the compressibility parameters interchanged for the soils. This resulted in a calibration for M1 sand with the compressibility of OS (called "M1B") and a calibration for OS with the compressibility of M1 (called "OSB"). Both simulations kept all model parameters the same as their original calibration while changing parameters ρ_c and σ_{vref} to the other soil type.

Changing the compressibility parameters affected the position of the CSL, as seen Fig. 9. The position of the LCCs reflected the change in compressibility – the less-compressible OS is to the right of the more-compressible M1 sand as expected, and the "B" calibrations interchange LCCs when they are assigned the other's compressibility. The CSLs of the "B" calibrations are positioned between the CSLs of original the M1 and OS calibrations.

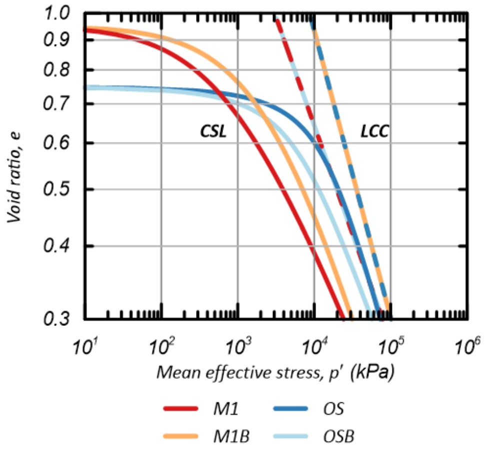

Figure 9. LCC and CSL of M1 and OS calibrations, M1 sand with OS ("M1B"), and OS with M1 compressibility ("OSB").

The simulated q_t values for the M1B and OSB calibrations are included in Fig. 7. Changes in compressibility did result in some change to q_t. The simulated q_t values of OSB were lower than the q_t values of OS for the same ξ, reflecting that OSB is more compressible than OS; however, they are only 15-25% lower than q_{tOS}, whereas q_{tM1} values are up to 60% lower. Similarly, q_{tM1B} values were larger than q_{tM1}, reflecting that M1B is less compressible than M1, however the values are only 10-20% larger. If compressibility indeed was the major factor in the q_t differences of OS and M1 sands, the change in q_t would be expected to capture the soil behaviour more closely with the same compressibility. These results indicate that compressibility differences do not fully account for differences in q_t for the same ξ between calcareous and silica sands.

It is likely and expected that changing compressibility parameters also changed the shear behaviour of the calibrations. This work does not examine these effects at this time but will be investigated in future studies. Particle size redistribution during CPT due to crushing also has been shown to influence q_t, CSL position and shear strength (Ciantia et al. 2016).

3.1.2. Role of CSL position on q_t

In this section, the second hypothesis that differences in q_t between M1 and OS relate to differences in CSL position is tested. The CSL position refers to the CSL position relative to p'. Therefore, the CSL position is captured in this study by the mean effective stress state ($\xi_{p'}$), which is the difference of p' between the initial p' and the p' on the CSL for the same initial e. The q_t values in Fig. 7 are related to $\xi_{p'}$ in Fig. 10 for M1 and OS. As shown in Fig. 10, there is a positive relationship between q_t and $\xi_{p'}$ for both soils, supporting that when the CSL is positioned at higher p', q_t will be higher. The data in Fig. 10 for OS and M1 show similar trends but different relationships between the two soils since other soil properties and behaviours will also affect q_t in addition to $\xi_{p'}$.

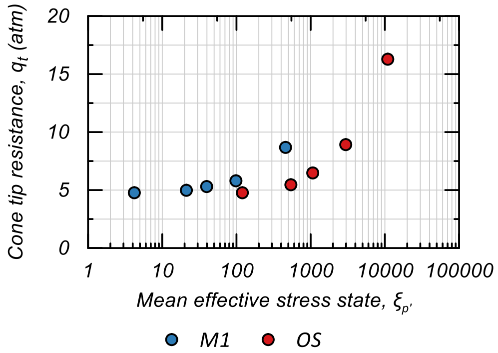

Figure 10. Relationship between q_t and $\xi_{p'}$ for OS and M1.

The relationship shown in Fig. 10 is consistent with the understanding that soils at the cone tip are loaded to the CSL during cone penetration (Moug et al. 2019b). To illustrate this in terms of CSL positioning, the CPT stress paths and CSLs for M1 sand and OS are shown in Fig. 11. The simulated loading paths show the e-p' response from initial conditions to the cone shoulder for soil along the cone's penetration path and then adjacent to the cone. Two simulations are shown for each sand, starting at the same ξ. All four simulations reach the CSL by the cone tip. Because the CSL of M1 is positioned to the left of OS (i.e., at lower p'), M1 soil at the cone tip is at a lower p' than OS soils, consequently, there is a lower q_t for M1.

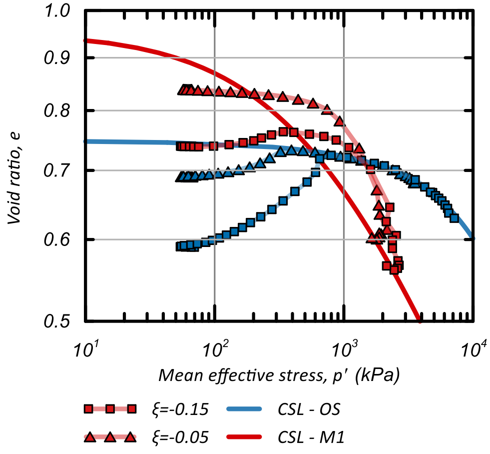

Figure 11. Stress paths during cone penetration and CSLs of M1 and Ottawa sands.

The relationship between q_{tOS}, q_{tM1} and CSL positions are further examined in Fig. 12. In this figure, the SCF for the simulated M1 soil is related to the ratio of p' on the CSL for OS and M1 for the same ξ. Each point in Fig. 12 has the same initial stress conditions (σ'_v = 100 kPa) and same ξ. The p'_{cs} values represent the p' values on the CSL for the same e that achieves the initial ξ at σ'_v = 100 kPa. As the differences in the horizontal position of the two CSLs become greater the ratio between q_t (the SCF) also increases. This relationship demonstrates that CSL position is a potential fundamental basis for a SCF.

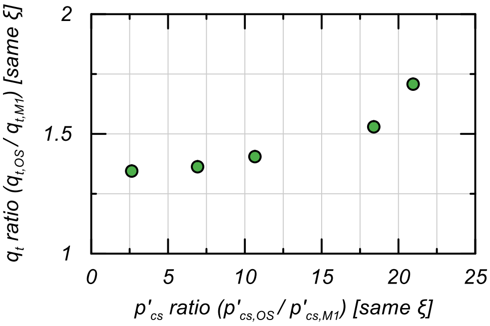

Figure 12. q_t ratio versus p' ratio of M1 and Ottawa sand simulations at same ξ and at σ'_v = 100 kPa.

4. Discussion

Numerical simulations of direct cone penetration were used to investigate differences in q_t between calcareous and silica sands. A consistently lower q_t in calcareous sands compared to silica sands at the same *Dr* or ξ is not fully attributable to differences in compressibility. However, there does seem to be a strong relationship between CSL position and q_t, and the differences in q_t can be explained by differences in CSL position in terms of p'. Relating these may provide a fundamental basis for SCFs.

Current approaches to developing SCFs are site-specific and based on a series of calibration chamber or centrifuge testing to estimate the differences in q_t for calcareous sands, requiring significant testing and time resources. The analysis presented herein shows that the differences in q_t between calcareous and silica sands are strongly related to the differences in their CSL positions with respect to p'. This may provide a basis for examining SCF in terms of the CSL position of the calcareous sand compared against a CSL representative of typical silica sands (i.e., the sands used to develop q_t-*Dr* relationships). Essentially, a SCF could be estimated by characterizing the calcareous sand CSL.

Such an approach could be an alternative to calibration chamber or centrifuge testing to develop SCF. However, a CSL-based approach to developing SCFs requires further investigation accompanied by experimental validation.

5. Conclusions

A direct axisymmetric penetration model calibration for calcareous sands was used to examine the role of compressibility on cone q_t and the relationship between the CSL and q_t. The study compared penetration simulations with the MIT-S1 model calibrated for a calcareous sand and a silica sand. The simulated q_t between the two calibrations indicates that the differences in q_t are only partially attributed to differences in compressibility, although differences in compressibility have been previously used to explain differences in q_t between calcareous and silica sands. A stronger explanation for the difference in simulated q_t between the calcareous sand and silica sand is the CSL positions. Examination of the role of CSL position on q_t could provide a path forward for development of SCF based on CSL characterization for calcareous sands.

Acknowledgements

The authors are grateful to Daniela Giretti for sharing lab results and supplemental data from their 2018 papers, and Portland State University for financial support.

References

Al-Homoud, A., & Wehr, W. "Experience of vibrocompaction in calcareous sand of UAE", Geotechnical & Geological Engineering, 24, pp. 757-774, 2006.

Boulanger, R. W., & Idriss, I. M. “CPT-based liquefaction triggering procedure”, Journal of Geotechnical and Geoenvironmental Engineering, 142(2), 2016.

Ciantia, M., Arroyo, M., Butlanska, J., & Gens, A. “DEM modelling of cone penetration tests in a double-porosity crushable granular material”, Computers and Geotechnics, 73, 109–127, 2016.

Ciantia, M., Arroyo, M., O’Sullivan, C., Gens, A., & Liu, T. “Grading evolution and critical state in a discrete numerical model of Fontainebleau sand”, Géotechnique, 1–15, 2018.

Debats, J., Pardessus, N., Racinais, J., & Olgun, C. “In-situ determination of the shell correction factor in carbonate sands”, In: 6th International conference on earthquake geotechnical engineering, Christchurch, New Zealand, 2015.

Giretti, D., Fioravante, V., Been, K., & Dickenson, S. “Mechanical properties of a carbonate sand from a dredged hydraulic fill”, Géotechnique, 68(5), 410-420, 2018a.

Giretti, D., Been, K., Fioravante, V., and Dickenson, S. "CPT calibration and analysis for a carbonate sand", Géotechnique, 68(4), 345-357, 2018b.

Jamiolkowski, M. & Pasqualini, E. “Compaction of granular soils: remarks on quality control”, Proceedings of Conference on Grouting, Soil Improvements and Geosynthetics, New Orleans, LA 25-28 Feb.

Mayne, P. Cone Penetration Testing State-of-Practice. NCHRP Project 20-05: Transportation Research Board Synthesis Study, 2007.

Moug, D., Price, A., Bastidas, A., Darby, K., Boulanger, R., & DeJong, J. "Mechanistic development of CPT-based cyclic strength correlations for clean sand", Journal of Geotechnical and Geoenvironmental Engineering, 145(10), 2019a.

Moug, D., Boulanger, R., DeJong, J., & Jaeger, R. “Axisymmetric simulations of cone penetration in saturated clay”, Journal of Geotechnical and Geoenvironmental Engineering, 145(4), 2019b.

Pestana, J., & Whittle, A. “Compression model for cohesionless soils”, Geotechnique, 45(4), 611-631.

Pestana, J., & Whittle, A. “Formulation of a unified constitutive model for clays and sands”, International Journal for Numerical and Analytical Methods in Geomechanics, 23(12), 1215-1243, 1999.

Salgado, R., Mitchell, J., & Jamiolkowski, M. “Calibration chamber size effects on penetration resistance in sand”, Journal of Geotechnical and Geoenvironmental Engineering, 124(9), 878-888, 1998.